Proceedings of IMECE'03
2003 ASME International Mechanical Engineering Congress
Washington, D.C., November 15–21, 2003

IMECE2003-55300

Boundary Layer Solution for the Turbulent Swirling Decay Flow Through a Fixed Pipe: SBR at the Inlet

A. F. Najafi[1]
Center of Excellence in Energy Conversion
School of Mechanical Engineering
Sharif University of Technology
P.O. Box 11365/9567, Tehran, Iran

M. H. Saidi
Center of Excellence in Energy Conversion
School of Mechanical Engineering
Sharif University of Technology
P.O. Box 11365/9567, Tehran, Iran

M. S. Sadeghipour
Center of Excellence in Energy Conversion
School of Mechanical Engineering
Sharif University of Technology
P.O. Box 11365/9567, Tehran, Iran

M. Souhar
LEMTA-ENSEM, CNRS, UMR 7563 INPL
2 Avenue de la Forêt de Haye B. P.
160/54504,
Vandoeuvre Cedex, France

ABSTRACT

In this study the developing turbulent swirling pipe flow is investigated both numerically and analytically. Governing equations are derived accompanying the boundary layer assumptions. Uniform and solid body rotation (SBR) distributions are taken into account for the axial and tangential velocities at the inlet of the pipe, respectively. Beyond the boundary layers, the flow pattern is considered to be the potential flow. Making use of the fourth-order Runge-Kutta scheme, the numerical solution of the differential equations is obtained. Further more, by simplifying the governing equations for large Rossby number, the analytical solution is performed. The results of numerical and analytical swirl intensity have been compared showing reasonable agreement. As an alternative solution, a CFD analysis has been done as well, having applied FLUENT software to support the ability of our methodology.

INTRODUCTION

Swirling flow is one of the most applicable and important fluid flow which occurs in numerous industrial applications such as spray nozzle, separator, cyclones and draft tube of the Francis and Kaplan turbines. Due to importance of this type of fluid flow, considerable research efforts have been perform in this regard.

One can mention several experimental works such as Yajnik and Subbaiah [1], Weske and Struve [2] and Kitoh [3].

In addition, several analytical and numerical studies have been done by Talbot [4], Weber [5], Taylor [6] etc. Regarding the swirling decay rate, most of the experimental and theoretical studies have been centered around it when a solid body rotation is superimposed on the developed flow. In this connection we can refer to the report of Talbot [4] for laminar and reports of Kitoh [3] and Steenbergen and Voskamp [7] for turbulent swirling decay pipe flow with an exponential decay rate in axial direction for the problem solution.

Although, numerous experimental studies have been performed, but due to swirling flow complications, particular attentions have been put on the CFD studies. In many cases these flows are turbulent. Therefore, the calculation of the Reynolds stresses in the momentum conservation equations requires a reliable turbulence model.

It is well known that the nature of swirling itself causes considerable degree of anisotropy in stress and dissipation tensors leading to a highly anisotropic eddy viscosity, [1,3]. Thus the classical $k-\varepsilon$ model which is the eddy-viscosity based model is not expectable to give reliable results. Kobayashi and Yoda [8] attempted to simulate numerically a swirling flow in a pipe by using the $k-\varepsilon$ model and indicated that the obtained velocity profiles were quite different from experimental data. They concluded that eddy viscosity components are anisotropic. They obtained satisfactory results by considering an anisotropic factor for eddy-viscosity.

[1] Visiting researcher, LEMTA-ENSEM, CNRS, UMR 7563 INPL, France

Computations based on the Reynolds stress model for swirling jet, Gibson and Younis [9] and for a swirling flow within two concentric cylinders, Hirai et al. [10], show good appearances in predicting the flow.

Hirai et al. [11] analyzed an axially rotating pipe flow using $k-\varepsilon$, modified $k-\varepsilon$ and RSM models. They observed that the results of the modified $k-\varepsilon$ model gave better performance than the $k-\varepsilon$ model and the mentioned results were comparable with the RSM results. In their modified model they applied Richardson number [12] to take into account the effects of the curvature streamline. Armifield [13] used additional term to modify the ε equation. Spall and Ashby [14] simulated a turbulent swirling flow inside both a diverging and a constant radius tube to predict vortex breakdown. They found that the RSM is better than the $k-\varepsilon$ model.

Generally in a swirling decay pipe flow, the structure of the tangential velocity profile can be classified into three regions, namely core, annular and wall regions. In the core region which is characterized by a forced vortex motion, the flow is laminarized and turbulence is suppressed [15]. In the annular region, which is similar to the free vortex motion, the skewness of velocity is noticeable, so that the isotropy hypothesis for turbulent viscosity does not work well and in the wall region the skewness of the flow becomes weak [3].

Even though, there are some research works relating to the swirling pipe flow, however majority of them have focused on fully developed swirling flow and not on the developing region.

In this analysis, the boundary layer solution for the turbulent swirling decay pipe flow is investigated. At the inlet of the pipe, for the axial and tangential velocities, uniform and solid-body rotation (SBR) distributions are taken into account, respectively. The fluid flow from the pipe inlet is assumed to be completely turbulence. Considering these assumptions at the pipe inlet region may not be fully realistic but it can be justified from the point of view of flow behaviour simplifications for some conditions. The CFD calculation verifies closely the above mentioned assumptions.

Applying the boundary layer momentum integrals, governing equations are derived. There are two differential equations and three unknowns, namely axial boundary layer thickness, tangential boundary layer thickness and angular velocity out of the boundary layer. The third differential equation can be derived from the combination of the continuity and tangential momentum equations far enough from the pipe wall. Making use of the fourth-order Runge-Kutta scheme, the solutions of the differential equations are obtained with the suitable boundary conditions.

NOMENCLATURE

$E=(\delta_z/\delta_\theta)^{1/7}$	one-seventh power of the axial/tangential boundary layer thickness
$\dot{M}$	momentum flux
R	pipe radius
$Ro=\frac{W_o}{R\omega}$	Rossby Number
S	swirl intensity
W_o	mean axial velocity
$W_{\delta_z}, V_{\delta_\theta}$	core axial and tangential velocities
$\dot{m}$	mass flow rate
p	static pressure
r,θ,z	coordinates
w,v	axial and tangential velocities
y	wall distance

Greek

ω	angular velocity
δ_1	displacement thickness
$\overline{\theta}$	momentum thickness
δ_z, δ_θ	boundary layer thicknesses along z and θ directions
$\tau_{wz}, \tau_{w\theta}$	axial and tangential wall shear stresses
ν	kinematic viscosity

Subscript

B	top of the control volume
in	inlet of the control volume
out	outlet of the control volume
$anal$	analytical solution

1 GOVERNING EQUATIONS

Two control volumes for axial and tangential directions are considered near the pipe wall. Applying the integral method for each control volume and considering the boundary layer approximations, governing equations are derived. The velocity normal to the pipe wall is assumed negligible as compared with the other velocity components.

Approximate velocity profiles inside the boundary layers are based on the 1/7th power distribution and out of the boundary layers, the axial and tangential velocity components are uniform and solid body rotation type, respectively.

$$y \le \delta_z \Rightarrow \frac{w}{W_{\delta_z}} = \left(\frac{y}{\delta_z}\right)^{1/7};\ y > \delta_z \Rightarrow W = W_{\delta_z} \qquad (1)$$

$$y \le \delta_\theta \Rightarrow \frac{v}{V_{\delta_z}} = \left(\frac{y}{\delta_\theta}\right)^{1/7};\ y > \delta_\theta \Rightarrow V_{\delta_\theta} = (R-\delta_\theta)\omega \approx R\omega \qquad (2)$$

1.1 CONTINUITY EQUATION

Employing the continuity equation for a control volume, starting at the entrance and ending at a desired axial position at the developing region, and considering the 1/7th power and

uniform flow for the axial velocity distribution inside and outside of the boundary layer, respectively, we follow up with:

$$W_o \pi R^2 = W_{\delta_z} \pi (R-\delta_z)^2 + \int_0^{\delta_z} 2\pi\, wR\, dy \tag{3}$$

Substituting Eq. (1). into Eq. (3). and integrating the integral term with respect to *y*, we obtain:

$$W_o = W_{\delta_z}(1-\frac{1}{4}\frac{\delta_z}{R}+\frac{\delta_z^2}{R^2}+...) \tag{4}$$

Since $\frac{\delta_z}{R} \approx O(0.1)$, then the above expression can be simplified as:

$$W_{\delta_z} \approx W_o(1+\frac{1}{4}\frac{\delta_z}{R}) \tag{5}$$

1.2 MOMENTUM EQUATIONS

Figure 1. represents typical axial and tangential control volumes. The momentum equation in the axial direction can be derived as:

$$\dot{M}_{out_z} - \dot{M}_{in_z} - \dot{M}_{B_z} = -\int_0^{\delta_z} \frac{dp}{dz} dz\, r\, d\theta\, dy - \tau_{wz} R d\theta\, dz \tag{6}$$

$$\dot{M}_{in_z} = \int_0^{\delta_z} \rho\, w^2 r\, d\theta\, dy \tag{7}$$

$$\dot{M}_{out_z} = \int_0^{\delta_z} \rho\, w^2 r\, d\theta\, dy + \frac{d}{dz}[\int_0^{\delta_z} \rho\, w^2 r\, d\theta\, dy]dz \tag{8}$$

$$\begin{aligned} \dot{M}_{B_z} &= \dot{m}_{B_z} W_{\delta_z} \\ \dot{m}_{B_z} &= \dot{m}_{out_z} - \dot{m}_{in_z} = \frac{d}{dz}[\int_0^{\delta_z} \rho\, w r\, d\theta\, dy]dz \\ \dot{M}_{B_z} &= W_{\delta_z} \frac{d}{dz}[\int_0^{\delta_z} \rho\, w r\, d\theta\, dy]dz \end{aligned} \tag{9}$$

$$\begin{aligned} &\frac{d}{dz}[\int_0^{\delta_z} \rho\, w^2 r\, d\theta\, dy]dz - W_{\delta_z} \frac{d}{dz}[\int_0^{\delta_z} \rho\, w r\, d\theta\, dy]dz \\ &\qquad = -\int_0^{\delta_z} \frac{dp}{dz} dz\, r\, d\theta\, dy - \tau_{wz} R d\theta\, dz \end{aligned} \tag{10}$$

It should be noted that the axial shear stress out of the boundary layer thickness is negligible.

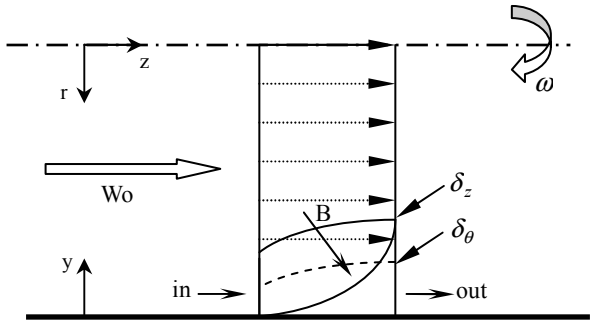

Figure 1. Typical axial and tangential control volume

Since the free stream or core region is taken to be moving with $r\omega$ around the pipe axis, there is a radial pressure gradient out of the boundary layer. A radial pressure gradient inside the boundary layer must be existed as well to keep the flow in circular path around the pipe axis. Most of the literatures [5,6,16], have considered a constant pressure inside the boundary layer, having these assumptions that both the boundary layer thickness compared with the pipe radius and radial pressure gradient are small as well.

In this study, since the type of swirling is solid body rotation and fluid is in turbulent regime, for a specified Reynolds and Rossby numbers, one may expect to have very large angular velocity. So, the radial pressure gradient may be considerable [17]. Consequently, considering the small boundary layer thickness with respect to the pipe radius, the radial pressure gradient will be:

$$-\frac{dp}{dy} \approx \rho R\omega^2 \tag{11}$$

Integrating Eq. (11). respect to *y* and considering the pressure at the edge of the axial boundary layer as the known boundary condition, we come up with the following relation:

$$p = p_{\delta_z} + \rho\omega^2 R(\delta_z - y) \tag{12}$$

The axial pressure gradient can be derived making derivative with respect to the *z* direction from the Eq. (12).:

$$-\frac{dp}{dz} = -\frac{dp_{\delta_z}}{dz} - \rho R \frac{d}{dz}(\omega^2(\delta_z - y)) \tag{13}$$

where the axial pressure gradient on the edge of the boundary layer can be obtained as:

$$-\frac{dp_{\delta_z}}{dz} = \rho \frac{1}{2}\frac{d}{dz}(W_{\delta_z}^2 + R^2\omega^2) \tag{14}$$

Substituting Eq. (14). into Eq. (13). and combining with Eq. (10)., the axial momentum equation is obtained as:

$$\frac{d}{dz}(W_{\delta_z}^2\bar{\theta})+W_{\delta_z}\frac{dW_{\delta_z}}{dz}\delta_1 - \left\{\int_0^{\delta_z} R^2\omega\frac{d\omega}{dz}dy - R(\delta_z^2\omega\frac{d\omega}{dz}+\omega^2\delta_z\frac{d\delta_z}{dz})\right\}=\frac{\tau_{wz}}{\rho} \quad (15)$$

where $\delta_1=\frac{1}{8}\delta_z$ and $\bar{\theta}=\frac{7}{72}\delta_z$.
The manipulation of Eq. (15). results in:

$$\left\{\begin{array}{l}\frac{23}{288}(W_{\delta_z}W_o\delta_z)+\frac{7}{72}W_{\delta_z}^2 \\ +16\,\omega_o^2R^3(\frac{R\delta_z}{(4R+\delta_z)^3}+\frac{\delta_z}{(4R+\delta_z)^2})\end{array}\right\}\frac{d\delta_z}{dz}=\frac{\tau_{wz}}{\rho} \quad (16)$$

The procedure to obtain the tangential momentum equation is the same as axial direction. So, it follows:

$$\frac{d}{dz}[\int_0^{\delta_\theta}\rho\,wvr^2\,d\theta\,dy]dz - V_{\delta_\theta}(R-\delta_\theta)\frac{d}{dz}[\int_0^{\delta_\theta}\rho\,w\,r\,d\theta\,dy]dz=-\frac{\tau_{w\theta}}{\rho}Rd\theta\,Rdz \quad (17)$$

The simplified forms of the tangential momentum equation are given for the following two cases:
If $\delta_\theta<\delta_z$ then:

$$\frac{d}{dz}[\frac{7}{9}V_{\delta_\theta}W_{\delta_z}\delta_zE^{-8})-V_{\delta_\theta}\frac{d}{dz}[\frac{7}{8}W_{\delta_z}\delta_zE^{-8}]=-\frac{\tau_{w\theta}}{\rho} \quad (17.1)$$

and if $\delta_z<\delta_\theta$

$$\frac{d}{dz}\left\{V_{\delta_\theta}W_{\delta_z}\delta_z(\frac{7}{8}E^{-7}-\frac{7}{72}E)\right\} - V_{\delta_\theta}\frac{d}{dz}\left\{W_{\delta_z}\delta_z(E^{-7}-\frac{1}{8})\right\}=-\frac{\tau_{w\theta}}{\rho} \quad (17.2)$$

The axial and tangential components of the shear stresses at the wall are required in Eqs. (16). and (17). It should be mentioned that, in turbulent flow the wall shear stress can not be obtained by using velocity gradient. Therefore, an empirical expression based on the Blasius law for the 1/7th power velocity distribution is used [18].

In order to evaluate two wall shear stresses the behaviour of the total velocity near the wall is used. Considering flow direction near the pipe wall and doing algebraic simplifications, axial and tangential shear stresses can be derived as follow:

$$\tau_{wz}=0.0225\rho W_{\delta_z}(W_{\delta_z}{}^2+V_{\delta_\theta}^2E^2)^{3/8}(\frac{\nu}{\delta_z})^{1/4} \quad (18)$$

$$\tau_{w\theta}=0.0225\rho V_{\delta_\theta}E(W_{\delta_z}{}^2+V_{\delta_\theta}^2E^2)^{3/8}(\frac{\nu}{\delta_z})^{1/4} \quad (19)$$

There are three unknowns namely δ_z, E and ω and only two equations. The third differential equation can be derived from the combination of the continuity and tangential momentum equations in far from the wall region, where the flow can be considered as inviscid. It follows:

$$W_{\delta_z}\frac{\partial\omega}{\partial z}=-\omega\frac{\partial W_{\delta_z}}{\partial z} \quad (20)$$

Putting Eq. (5). into Eq. (20). and making integration with respect to z, a relation for the angular velocity of the free stream, ω, can be obtained.

$$\omega\approx\omega_o(1+\frac{1}{4}\frac{\delta_z}{R})^{-1} \quad (21)$$

As the angular velocity is derived analytically, the boundary conditions for the remaining two differential equations are as follow:

$$\begin{array}{l} z=0;\ \ \delta_z=0 \\ z=0;\ \ E=1.0\end{array} \quad (22)$$

Since Eqs. (16). and (17). are identically infinity at $z=0$, thus we should have another approach for our estimation of the results nearly the pipe inlet. In this regard, the boundary layer thickness is estimated by $\alpha z^{4/5}$ (see, for example, [5]) and the value of E equal unity at the above region.

2 RESULTS OF NUMERICAL SOLUTION

The numerical solution for the governing equations is performed using the fourth-order Runge-Kutta scheme.

To study the effect of the swirl on the fluid flow behaviour, several calculations are performed considering a mean axial velocity and several Rossby numbers. Figure 2. shows the dimensionless core axial velocity for several Rossby numbers. As it is shown, increasing the Rossby number, the dimensionless core axial velocity will be increased. It is obvious that in swirling flow, the decay of swirl in the pipe leads to decay in the radial pressure gradient. Consequently, the axial pressure gradient along the pipe axis may decrease more than would be the case for non-swirling flow [13]. As the pressure gradient decreases, the axial velocity gradient along the pipe axis should be decreased. The above mentioned expression is confirmed by the results of Fig. 2.

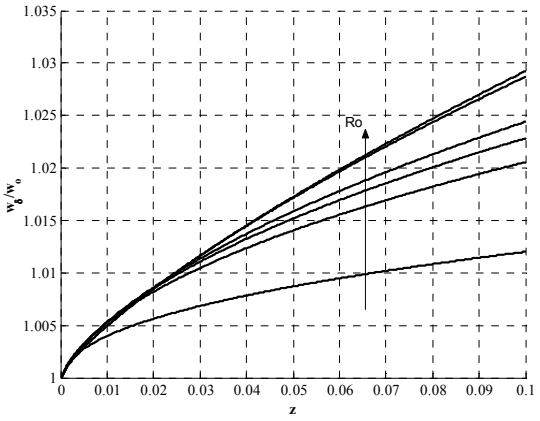

Figure 2. Distribution of dimensionless axial velocities along the pipe axis

Figures 3. and 4. show the axial and tangential shear stresses along the pipe wall. As it is expected, the axial and tangential shear stresses are decreased along the pipe wall since the boundary layer thickness increases and swirl intensity decreases. Meanwhile, these two parameters are decreased by increasing the Rossby number.

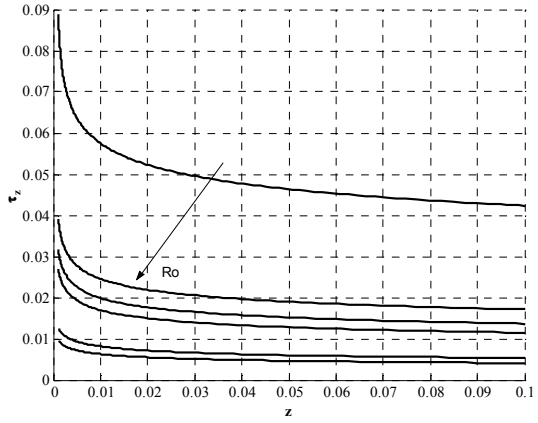

Figure 3. Axial wall shear stress along the pipe wall

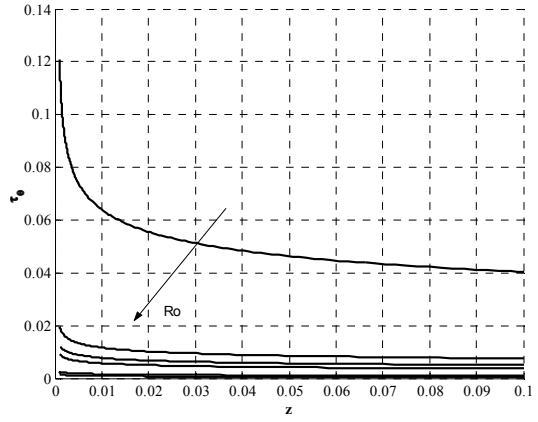

Figure 4. Tangential wall shear stress along the pipe wall

3 RESULTS OF ANALYTICAL SOLUTION

Parametric studies of different terms of the axial momentum equation are necessary to find out the nature and variation of them with respect to different Rossby numbers.

Focusing on the left hand side of the Eq. (16). and using the boundary layer solution, it can be rearranged as:

$$LHS : W_o^2 \left[\underbrace{\frac{37}{288}\frac{\delta_z}{R}}_{a} + \underbrace{\frac{7}{72}}_{b} + \underbrace{\frac{5}{4} Ro^{-2} \frac{\delta_z}{R}}_{c} \right] \frac{d\delta_z}{dz} \qquad (23)$$

The right hand side of the Eq. (16). can be reformulated in more simple form as:

$$RHS : \ 0.0225 W_o^{7/4} (1 + \frac{\delta_z}{2R}) \underbrace{(1 + E^2 R_o^{-2})^{3/8}}_{d} (\frac{\nu}{\delta_z})^{1/4} \qquad (24)$$

Considering the large Rossby numbers, the term *c* can be neglected with respect to the term *a*. On the other hand we realize that at high Reynolds number or at the pipe inlet, the boundary layer thickness is so small relative to the pipe radius. Consequently, the term *a* is negligible compared to the term *b*.

Figure 5. shows the variation of term *d* along the *z* axis for different Rossby numbers. It can be seen that increasing the Rossby number causes the value of term *d* to approach to one.

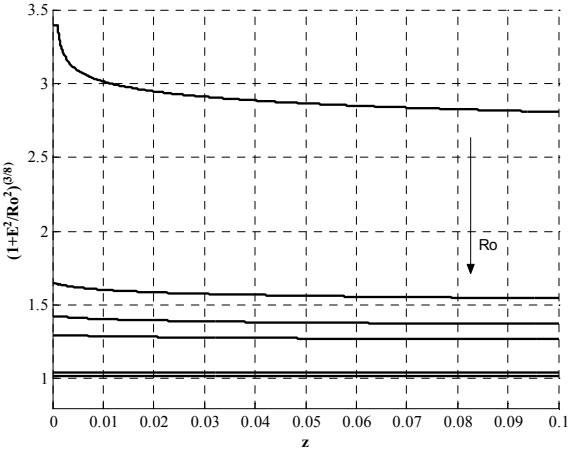

Figure 5. Variation of term *d* in Eq. (24). along the pipe axis

In order to derive a relation between δ_z and z, Eqs. (23). and (24). are manipulated, simplified and integrated to give:

$$3.45744 (\frac{W_o}{\nu})^{1/4} \delta_z^{5/4} = z \rightarrow \delta_z \approx 0.37 (\frac{W_o}{\nu})^{-1/5} z^{4/5} \qquad (25)$$

The above expression is similar to the relation for the turbulent flat plate, which is expectable since we consider high Rossby number and very small boundary layer thickness.

In swirling internal pipe flow it is important to realize the swirl decay rate along the pipe axis. Thus the swirl intensity should be defined in advance. The swirl intensity for axis-symmetric flow is defined as [7]:

$$S = \frac{2}{R^3 W_o^2} \int_0^R wvr^2 dr \qquad (26)$$

This may be broken down into:

$$S = \frac{2}{R^3 W_o^2} \left[\int_0^{R-\bar{a}} wvr^2 dr + \int_{R-\bar{a}}^{R-\bar{b}} wvr^2 dr + \int_{R-\bar{b}}^{R} wvr^2 dr \right] \qquad (27)$$

where $\bar{a}$ and $\bar{b}$ may be replaced by δ_z and δ_θ. The swirl intensity for each situation can be calculated using the above expression.

In order to derive an analytical relation for the swirling decay rate using the Eq. (27)., we should generally have both δ_z and δ_θ. The first term has been approximated considering appropriate assumptions. The second term must be derived from the Eq. (17). which is too complicated. As an approximate estimation of the δ_θ, we may go back to numerical solution. Figure 6. shows that for the large Rossby numbers, the ratio of the boundary layer thicknesses are approximately unity.

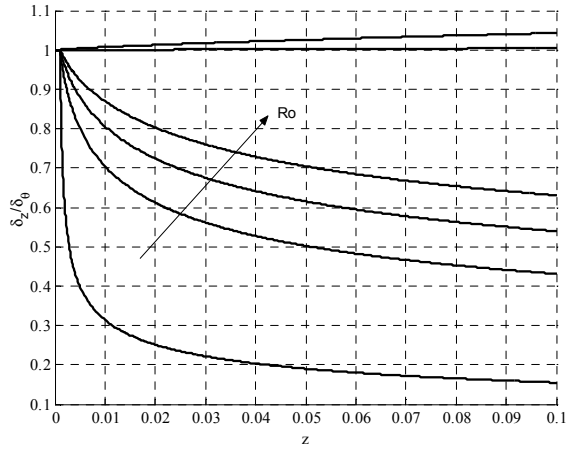

Figure 6. Ratio of axial to tangential boundary layer thickness w.r.t. the pipe axis

Simplification of Eq. (27)., considering previous assumptions leads to analytical swirl intensity formulation as:

$$S_{anal} = \frac{R_o^{-1}}{2}\left(1 - \frac{8}{9}\frac{0.37\left(\frac{W_o}{\nu}\right)^{-1/5} z^{4/5}}{R}\right) \qquad (28)$$

Equation (28). represents analytical swirling decay rate for developing swirling pipe flow.

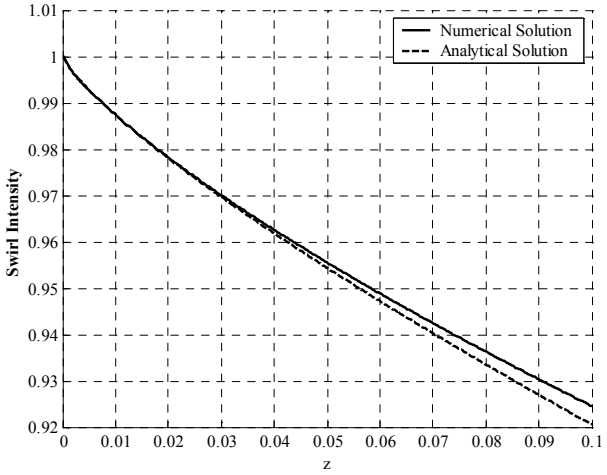

Figure 7. Swirling decay rate, numerical and analytical solutions; Wo=5 m/s, Ro=5

The results of analytical and numerical solutions are shown in Fig. 7. The analytical result is based on the Eq. (28). The deviation from numerical results at large axial distance is due to lack of compatibilities of basic assumptions in deriving the analytical formulation for the swirl decay rate.

4 RESULTS OF CFD SIMULATION

In this research, CFD simulation is used to support the ability of our numerical approach. In this regard, the FLUENT software has been employed. Considerable attention has been paid to find out the most reliable approach to model the Reynolds stresses for this type of flow.

In this regard, the Reynolds stresses in Navier-Stokes equations are modeled by using RSM formulation. Figure 8. shows the dimensionless axial velocity obtained from the numerical and CFD calculations.

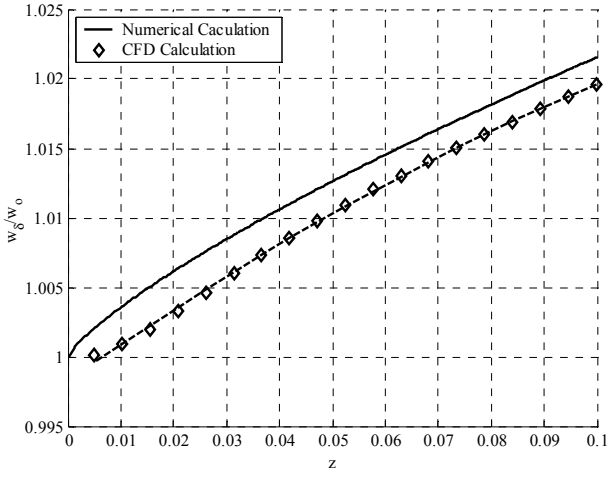

Fig. 8. Distribution of dimensionless axial velocity, numerical and CFD calculations; Wo=5 m/s, Ro=5

Considering CFD calculation, the pipe length has been considered very large to ensure fully developed flow at the outlet. Figure 8. shows that at far enough from the pipe inlet, two results of numerical and CFD calculations converge. Assumption of turbulent flow condition just at the pipe inlet is not exact, as the flow regime should pass from laminar and transient to turbulent regime. It should be noted that both numerical and CFD calculations have some weaknesses, since they are not capable of capturing simultaneously laminar, transient and turbulent zones. In addition, the axial velocity may be affected by the swirling velocity at the pipe inlet. However the results of CFD calculation seems to be more realistic than the numerical solution, as it solves full Navier-Stokes equations.

Therefore, the CFD approach has the capability of capturing the above mentioned flow behaviour. The positional lag between CFD and numerical calculations at Fig. 8. is due to this difference in calculation scheme.

Consequently, it seems that for high Reynolds and Rossby numbers both numerical and CFD simulations will be reliable since the entrance effects are dominated.

Figure 9. shows error analysis of the results of swirl intensity decay rate for CFD and numerical calculations as well.

As it is seen the difference between these two results fall into ± 5 % which is well acceptable.

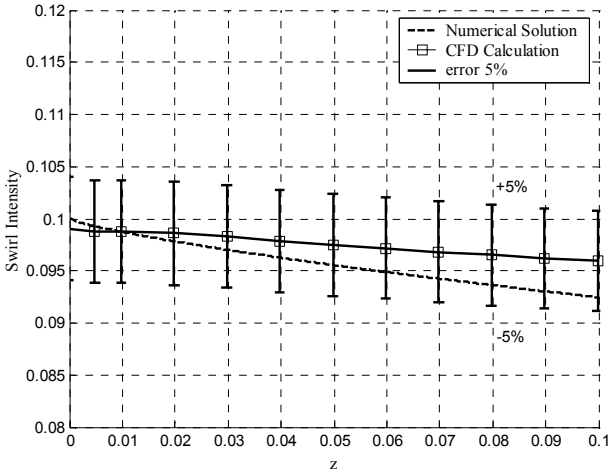

Figure 9. Swirling intensity decay rate, comparison with CFD calculation; W_o=5 m/s, Ro=5

5 CONCLUSIONS

So far, in this research three methods of analysis were implemented to model the developing turbulent swirling decay pipe flow. Numerical solution applying the fourth-order Runge-Kutta scheme shows that this method is well applicable at both high Reynolds and Rossby numbers which leads to reasonable results.

Analytical solution for large Reynolds and Rossby number follows up properly the numerical solution except for large distance from the pipe inlet which shows a rather deviation.

CFD simulation results support the validity and domain of the results of the numerical scheme, except for a narrow entrance region where there is a positional lag between two schemes.

The positional lag between CFD and numerical calculations at Fig. 8. is due to difference in formulations of these two methods.

It is concluded that the results of CFD calculations are more realistic since the full Navier-Stokes equations are solved in this concern. We must realize that the assumption of turbulent flow condition just at the pipe inlet is not exact as the flow regime should pass from laminar and transient to turbulent regime.

We may rely on the results of analytical solution at high Reynolds and Rossby numbers since this method of analysis shows cost effective performance than numerical and CFD solutions.

Error analysis of the swirl intensity results of CFD and numerical calculations has been performed. The difference between these two results is shown in Fig. 9. which falls into ± 5 % being well acceptable in swirl intensity decay rate.

6 REFERENCES

[1] Yajnik, K., S., and Subbaiah, M., 1973, "Experiments on Swirling Turbulent Flow. Part 1. Similarity in Swirling Flows," J. Fluid Mech., **60**, pp. 665-687.

[2] Weske, D. R., and Struve, G. YE., 1974, "Experimental Study of Turbulent Swirled Flows in a Cylindrical Tube," FLUID MECHANICS-Soviet Research, **3**(1), pp. 77-82.

[3] Kitoh, O., 1991, "Experimental Study of Turbulent Swirling Flow in a Straight Pipe," J. Fluid Mech., **225**, pp. 445-479.

[4] Talbot, L., 1954, "Laminar Swirling Pipe Flow," Journal of Applied Mechanics, **21**, pp. 1-7.

[5] Weber, H., E., 1956, "The Boundary Layer Inside a Conical Surface Due to Swirl," Journal of Applied Mechanics, **23**, pp. 587-592.

[6] Taylor, G., H., 1949, "The Boundary Layer in the Converging Nozzle of a Swirl Atomizer," Quart. J. Mech. and Applied Math., **3**, pp. 129-139.

[7] Steenbergen W., Voskamp J., 1998, "The Rate of Decay of Swirl in Turbulent Pipe Flow," Flow Measurement and Instrumentation, **9**, pp. 67-78

[8] Kobayashi, T. and Yoda, M., 1987, "Modified $k-\varepsilon$ Model for Turbulent Swirling Flow in a Straight Pipe," JSME. Int. J., **30,** pp. 259 66-71.

[9] Gibson, M. M. and Younis, B. A., 1986, "Calculation of Swirling Jets with a Reynolds Stress Closure," Phys. Fluids. **29(1)**, pp. 38-48.

[10] Hirai, S., Takachi, T., Tanaka, K. and Kida, K., 1987, "Effect of Swirl on the Turbulent Transport of Momentum in a Concentric Annular with a Rotating Cylinder," Trans. JSME. **B 53,** pp. 432

[11] Hirai, S., Takachi, T., Matsumoto, M., 1988, "Prediction of the Laminarization Phenomena in an Axially Rotating Pipe Flow," Trans., ASME J. Fluids Eng. **110**, pp. 424-430
[12] Bradshaw, P., 1969, "The Analogy Between Streamline Curvature and Buoyancy in Turbulent Shear Flow," J. Fluid Mech., **36,** pp. 177-191.
[13] Armfield, S., W. and Fletcher, C., A., J., 1989, "Comparison of and Algebraic Reynolds Stress Models for Swirling diffuser Flow," Int. J. for Numerical Methods in Fluids, **9**, pp. 987-1009.
[14] Spall, R. E. and Ashby, B. M., 2000, "A numerical study of Vortex Breakdown in Turbulent Swirling Flows," ASME, J. Fluids. Eng., **122**, pp. 179-183.
[15] Smirov, A. and Chomik, J., 1997, "Turbulent Swirl Flow Modeling," Technical Report, Dept. Thermo and Fluid Dynamics, Chalmers University of Technology, Göteborg, SWEDEN.
[16] Binnie, A., M., and Harris, D., P., 1949, "The Application of Boundary Layer Theory to Swirling Liquid Flow Through a Nozzle," Quart. J. Mech. and Applied Math., **3**, pp. 89-106.
[17] Akiyama, T., and Ikeda, M., 1986, "Fundamental Study of the Fluid Mechanics of Swirling Pipe Flow with Air Suction," Ind. Eng. Chem. Process Des. Dev., **25**, pp. 907-913.
[18] Schlichting, H., 1968, *Boundary Layer Theory,* McGraw-Hill, New York.